

Constraints on large-scale polarization in northern hemisphere

Dongdong Zhang,^{1,2,3} Bo Wang,^{1,2} Jia-Rui Li,^{1,2} Yi-Fu Cai,^{1,2,*} and Chang Feng^{1,2,†}

¹*CAS Key Laboratory for Research in Galaxies and Cosmology, Department of Astronomy, University of Science and Technology of China, Hefei, Anhui 230026, China*

²*School of Astronomy and Space Science, University of Science and Technology of China, Hefei 230026, China*

³*Kavli IPMU (WPI), UTIAS, The University of Tokyo, Kashiwa, Chiba 277-8583, Japan*

(Dated: August 2, 2024)

Present cosmic microwave background (CMB) observations have significantly advanced our understanding of the universe's origin, especially with primordial gravitational waves (PGWs). Currently, ground-based CMB telescopes are mainly located in the southern hemisphere, leaving an untapped potential for observations in the northern hemisphere. In this work, we investigate the perspective of a northern hemisphere CMB polarization telescope (NHT) to detect PGWs and present mock data for such a project. We forecast the detection sensitivity on the tensor-to-scalar ratio r of NHT and compare it with the existed ground-based experiments, also search for optimal experimental configurations that can achieve the best sensitivity of r . Our results indicate that, considering realistic experimental conditions, the first year of NHT observations combined with *Planck* can achieve a precision of $\sigma(r) = 0.015$, reaching the level of BICEP2/*Keck*, with significant potential for improvement with subsequent instrumentation parameter enhancements.

I. INTRODUCTION

Inflation theory is fundamental to modern cosmology, resolving several problems in Big Bang cosmology, such as the horizon, flatness, and monopole issues [1–7]. Furthermore, inflation predicts that quantum fluctuations in the inflaton field and spacetime produce scalar and tensor modes, leading to primordial perturbations. Scalar modes cause temperature anisotropies in the cosmic microwave background (CMB), which lead to the formation of large-scale structures [8–13]. On the other hand, tensor modes, also known as primordial gravitational waves (PGWs), left their imprint on the B-mode polarization of the CMB [14–16].

Over the past few decades, progress has been made toward understanding the universe's origins through long-term observations of the CMB. The *Planck* mission marked a critical milestone in this field, providing precise observations that ruled out the simplest model of power-law inflation [17, 18]. Ground-based CMB experiments [19–23] have also achieved even more precise measurements due to much lowered instrumental noise and sophisticated low-temperature detection techniques. Currently, the BICEP3/*Keck* experiment has achieved the best constraints on the tensor-to-scalar ratio r , with an upper bound of $r < 0.036$ (95%) [19]. However, a definitive detection of PGWs remains elusive, and researchers continue to search for these signals [24, 25]. The CMB polarization studies become an active area of research with considerable potential for uncovering new physics and broadening our understanding of the universe.

However, ground-based telescopes may suffer from complicated technical issues such as geographic locations and

sky-scanning strategies which can result in different sky coverage and levels of atmospheric contamination. To date, most ground-based CMB telescopes are located in the Southern Hemisphere, such as the Atacama desert and the south pole. The Northern Hemisphere would become another important observing location [26–29].

In this work, we constructed a generic mock survey for a futuristic Northern Hemisphere CMB Telescope (NHT). We investigated the detection sensitivity of PGWs with the NHT and examined the impact of instrumental configurations on the PGW detection sensitivity. These forecasts could become a guidance for the design of future NHT.

This paper is organized as follows: In section II, we introduce the instrument summary and the forecasting methodology used in our calculations. We present our forecast results and analyze the impact of various experimental parameters on the sensitivity of detecting PGWs in section III. Finally, we conclude in section IV.

II. METHODOLOGY

A. Instrument Summary

Ground-based CMB telescopes face a significant challenge: atmospheric molecules in the millimeter/sub-millimeter band absorb and emit signals, compromising data quality. Water vapor is particularly problematic due to its strong absorption properties and quick variability. Precipitable Water Vapor (PWV), which represents the total water depth in an atmospheric column above ground level, is typically used to quantify atmospheric water vapor. Given the faint nature of CMB signals, especially polarization signals, CMB observation sites must provide exceptionally clear, dry, and stable atmospheric conditions. According to MERRA-2 data on global mean PWV distribution from July 2011 to July 2016 [30, 31],

* Corresponding author: yifucai@ustc.edu.cn

† Corresponding author: changfeng@ustc.edu.cn

only Antarctica, the Atacama Desert, Greenland, and the high Tibetan Plateau exhibit minimal PWV levels. These regions are thus the most suitable for ground-based CMB telescopes.

Currently, all ground-based CMB telescopes are located in the southern hemisphere, primarily in Chile and Antarctica. No significant CMB data has been collected from the northern hemisphere. This situation is set to change with the advancement of Northern Hemisphere telescope projects like AliCPT and GreenPol. These projects aim to provide high-precision measurements of CMB polarization in the northern sky in the near future. For forecasting purposes, we designate these Northern Hemisphere Telescopes as NHTs. We generate mock data based on a power spectrum independent of specific pipeline methods. To evaluate the potential performance of NHTs, we employ the Markov Chain Monte Carlo (MCMC) method.

The design of a CMB telescope requires the meticulous selection of several parameters. The critical parameters selected for our hypothetical telescope encompass the survey area f_{sky} , the number of channels, the Full Width at Half Maximum (FWHM), and the noise level $w^{-1/2}$. We opted for two channels to monitor the 95 GHz and 150 GHz bands, with FWHM values of 19 arcmin and 11 arcmin respectively. The survey area f_{sky} is set at 0.1. The rationale behind the selected noise level will be discussed in the subsequent section.

B. Foreground

Since the foreground for surveys in the northern sky and the southern sky are different, establishing the NHT provides an excellent window for independent verification of signals that may be discovered in the future by southern telescopes.

Foreground contamination is a challenge that needs to be carefully considered for NHT. The galactic emissions, particularly thermal dust and synchrotron emission, are major contributors to the foreground signal that needs to be separated from the desired B-mode signal by the so-called ‘‘component separation’’ methods. These methods are usually divided into blind [32–36], parametric [37, 38], and template removal techniques [39–41].

Several studies have forecasted the performance of blind methods on B-mode mock data for some future experiments [42–45]. In the case of the northern hemisphere, previous studies also evaluated the performance of various pipeline methods in cleaning foregrounds, with residual foreground contamination at least an order of magnitude below noise for their designed experiments at the multipoles of interest ($\ell \lesssim 100$) for constraining r [46, 47]. Therefore, in our work, we safely neglect the residual foreground and focus on the impact of the main instrument parameters on the constraints of the tensor-to-scalar ratio r .

C. Noise Model

The modeling of our anticipated noise spectra contains the white noise and the $1/f$ noise component,

$$N_l = N_{\text{red}} \left(\frac{\ell}{\ell_{\text{knee}}} \right)^{\alpha_{\text{knee}}} + N_{\text{white}}. \quad (1)$$

The $1/f$ noise component, mainly from atmospheric and electronic noise, is represented by N_{red} , ℓ_{knee} , and α_{knee} . The white noise component is denoted by N_{white} . Using this noise model, it is estimated that a small-aperture ground telescope dedicated to large-scale CMB physics could have a noise model with $\ell_{\text{knee}} \approx 50$ and α_{knee} between -3.0 and -2.4 , describing the uncertainty in the B-mode power spectrum, as discussed in [48]. We adopt the assumption that $\ell_{\text{knee}} = 30$, $\alpha_{\text{knee}} = -2.5/-3.0$ for 95/150GHz, and we fix $N_{\text{red}} = N_{\text{white}}$, as shown in Fig. 1. In the polarization noise spectrum at 95 GHz, the $1/f$ noise unnaturally rises at high ℓ due to the exponential increase of N_{white} at high ℓ in the parameterization. However, this defect does not affect the calculation, as white noise dominates at high ℓ .

We refrain from modeling the $1/f$ noise on the TT spectrum, as our hypothetical experiment only involves a small aperture telescope, rendering the Large Aperture Telescope modeling scenario irrelevant. From a data perspective, we argue that this omission will not affect the actual observational results, as the TT spectrum has already been precisely measured by WMAP and *Planck*. From a physical standpoint, when using CMB to detect PGWs, the primary focus is on the BB polarization power spectrum, and there is no need to be concerned about this bias term in the noise model of the TT power spectrum. Even so, we will show in the calculation analysis later that for the polarization mode, the consideration of $1/f$ noise does not significantly affect the restrictions on PGWs.

To derive a reliable estimate of N_{white} , we draw from the findings of previous forecasts for northern hemisphere CMB experiments, which employed specific pipeline methods [46, 49, 50], with $\sigma(r) \approx 0.02$. The MCMC method, as explained in Section IID, is utilized to estimate the noise level with polarized modes $w_{\text{p}} = 40 \mu\text{K} \cdot \text{arcmin}$ for a single channel. Given that the hypothetical NHT has two channels, the final noise power spectrum should be computed according to Eq. 2. The resulting effective noise level aligns closely with [51], despite the variation in calculation methodology. We list the initial operating parameters of NHT (named NHT-1) in Table I.

Assuming statistical independence of the noise in temperature and polarization in the CMB power spectra, the white noise spectra in TT, EE, and BB for scenarios with

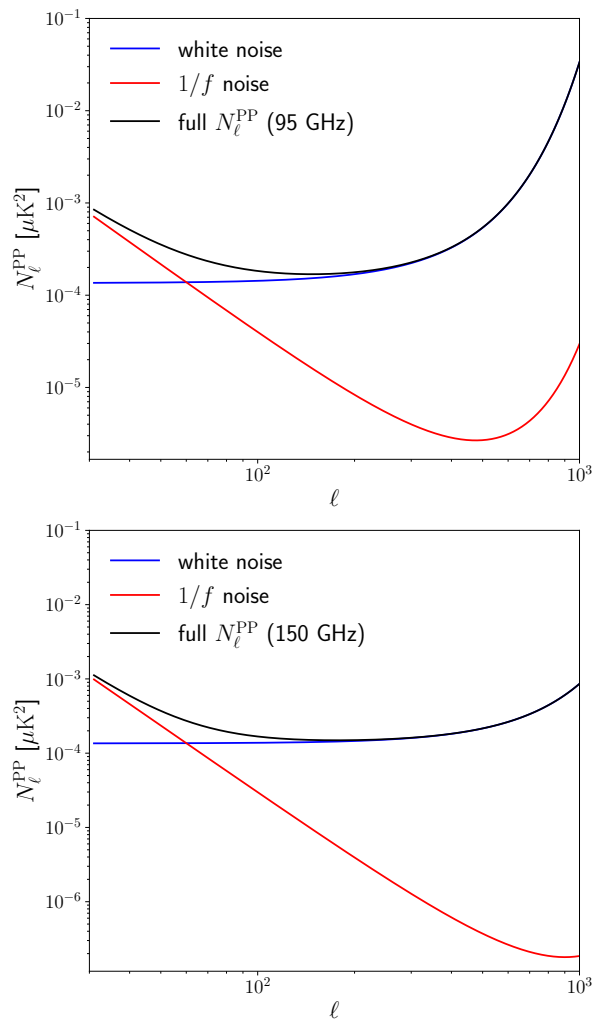


FIG. 1. The mock polarization noise power spectra of NHT-1. The black line is the total noise power spectrum that includes $1/f$ noise, and the red line is the power spectrum of white noise.

multiple channels are [52, 53]:

$$N_{\text{white}}^{\text{PP}} = \left(\sum_{\nu} w_{\text{P},\nu} \exp \left[-\ell(\ell+1) \frac{\theta_{\text{FWHM},\nu}^2}{8 \ln 2} \right] \right)^{-1}, \quad (2)$$

$$N_{\text{white}}^{\text{TT}} = \frac{1}{2} N_{\text{white}}^{\text{PP}}. \quad (3)$$

Here, $N_{\text{white}}^{\text{PP}}$ denotes the white noise spectra in EE and BB modes, and $N_{\text{white}}^{\text{TT}}$ denotes the white noise spectrum in TT mode. Based on the assumed parameters in Table I, the fiducial N_{ℓ}^{PP} power spectrum is shown in Fig. 1.

For the lensing reconstruction field, the quadratic estimation method is employed to calculate the error on the power spectrum, as detailed in [54]. The computations are implemented using the publicly accessible code, QuickLens[55]. Given the absence of real data in NHT, we utilize the mock spectra from *Planck*, provided in [56],

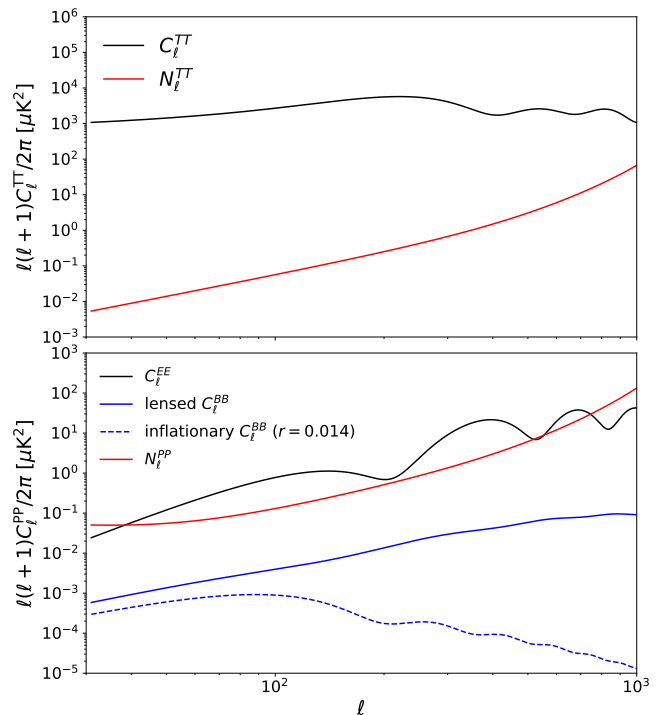


FIG. 2. Signal and noise on the temperature and polarization power spectra. Upper panel: The black line is signal of TT spectra, the red line is noise spectrum. Lower panel: The black line is signal of EE spectra, the blue solid/dot line is signal of lensed/inflationary spectrum, the red line is polarization noise spectrum.

for forecasting purposes.

Channels(GHz)	$w_{\text{P}}^{-1/2} (\mu\text{K} \cdot \text{arcmin})$	$\theta_{\text{FWHM}} (\text{arcmin})$	f_{sky}
95	40	19	0.1
150	40	11	0.1

TABLE I. Instrumental parameters for NHT-1.

D. Forecasting Procedure

With NHT's equipment parameters, we simulate the CMB TT, EE and BB power spectra as shown in Fig. 2. We use the best-fit parameters of *Planck* 2018 [17] which is shown in Table I and assume that the tensor to scalar r is 0.014 where the pivot scale k_* is selected as 0.05 Mpc^{-1} as our fiducial model based on the $\Lambda\text{CDM}+r$ model. We also forecast the joint NHT and *Planck* constraints on r for comparison with BICEP series.

ω_b	ω_{cdm}	θ_s
0.02242	0.11933	1.04101
$\ln 10^{10} A_s$	n_s	τ_{reio}
3.047	0.9665	0.0561

TABLE II. Fiducial cosmological parameters for mock NHT-1 power spectra.

The likelihood function we used is as follows

$$-2 \ln \mathcal{L} = \sum_{X=T,E,B} \sum_{\ell} \left(\frac{\hat{C}_{\ell}^{XX} - C_{\ell}^{XX}}{\Delta C_{\ell}^{XX}} \right)^2, \quad (4)$$

where \hat{C}_{ℓ}^{XX} are the mock power spectra, C_{ℓ}^{XX} are the fiducial power spectra, and the error term ΔC_{ℓ}^{XX} satisfy

$$\Delta C_{\ell}^{XX} \simeq \sqrt{\frac{2}{(2\ell+1)f_{\text{sky}}}} (C_{\ell}^{XX} + N_{\ell}^{XX}). \quad (5)$$

We utilize the publicly MCMC code Montepython [57, 58] and the publicly available Boltzmann code CLASS [59] to perform the calculations. We choose the Metropolis Hastings algorithm as our sampling method. For each model, we run MCMC calculation until $R-1$ for each fundamental parameter reach to the order of 0.001, according to the Gelman-Rubin criterion [60].

We choose $\ell_{\text{min}} = 30$ in order to consider the influence of PWV on the ground-based telescope follow the prescription in [53]. For ℓ_{max} , we estimate it to be the reciprocal of the best FWHM in the two channels. In our calculation, it is assumed that $\ell_{\text{max}} = 1000$.

This study presents a general discussion on the constraining power of NHT on PGWs and the improvement in detection capability following instrumental parameter optimization. Rather than focusing on specific pipeline construction methods, foreground separation techniques, atmospheric noise subtraction, or sky survey strategies, we concentrate on the direct influence of key experimental parameters on the observed CMB power spectra. This approach ensures our results provide generic guidance applicable to any future technical strategy adopted by NHT.

III. RESULT

After parameter estimation for NHT-1, we combined the NHT-1 data with a mock *Planck* 2018 dataset, utilizing the $\Lambda\text{CDM}+r$ model to compute the MCMC. This approach allows for a direct comparison with the results reported by BICEP series. Since our forecast for NHT uses a simulated power spectrum, it cannot be combined with real data in the Montepython program. Therefore, for computational convenience, we used the simulated *Planck* 2018 power spectrum developed by Brickmann [56]. The constraints of the simulated *Planck* dataset on

the cosmological parameters of the ΛCDM model differ by no more than 1% from the real *Planck* 2018 data.

For the primordial B-mode, we set the fiducial value to $r = 0.014$, consistent with the non-zero central value reported by BICEP3/*Keck* [19], to ensure a reliable comparison. Using the NHT-1 only to constrain r , we obtain its constraint sensitivity as $\sigma(r) = 0.023$.

In the data combination process, we replace the CMB TT, EE, and BB power spectra of mock *Planck* in the range of $l = 30 - 1000$ with those from NHT-1, corresponding to a 10% sky coverage. More specifically, in the joint computation, we used low- ℓ data ranging from $\ell = 2 - 29$ with a *Planck* precision and f_{sky} of 0.57, data ranging from $\ell = 30 - 1000$ with an NHT-1 precision and f_{sky} of 0.1, data ranging from $\ell = 30 - 1000$ with a *Planck* precision and f_{sky} of 0.47, and high- ℓ data ranging from $\ell = 1001 - 3000$ with a *Planck* precision and f_{sky} of 0.57. These experimental parameters are shown in Table III. In Fig. 3 to Fig. 6, we plot the power spectrum of each dataset. The joint calculation shows $\sigma(r) = 0.015$. We present in Fig. 7 a comparison of the sensitivity of constraints on r from NHT-1 only and NHT-1 combined with *Planck*. This result shows that the constraining accuracy of NHT-1 + *Planck* 2018 on PGWs can be better than the results of BICEP2/*Keck* + *Planck* 2015 [61], $\sigma(r) < 0.020$.

To study the impact of red noise in the noise model, we removed the red noise term in Eq. 1 and calculated the forecast on $\sigma(r)$ using only NHT-1. In this case, $\sigma(r) = 0.019$. Figure 8 shows the forecast for the constraint of r by NHT-1, with and without $1/f$ noise.

Furthermore, we explore how certain instrument parameters can enhance the ability to constrain PGWs. In the previous calculation, we assumed that the ℓ range is $30 < \ell < 1000$ for NHT as discussed in Section IID. Considering that the actual construction of the instrument may be inconsistent with our assumptions during the real observation, we evaluated the impact of changing the boundary conditions of ℓ_{min} on constraining PGWs. The calculation results are listed in the Fig. 9, which shows that changing ℓ_{min} from 30 to 70 has a notable influence on the $\sigma(r)$ from 0.021 to 0.037. This shows that low- ℓ polarization mock data greatly affects $\sigma(r)$, indicating that stringent atmospheric noise removal techniques are crucial for improving NHT's ability to constrain PGWs. Regarding ℓ_{max} , increasing the telescope aperture and thereby reducing FWHM can increase ℓ_{max} . However, since when detecting PGWs, the power spectrum region we concern about is $\ell \lesssim 100$, the construction of a large-aperture telescope is not suitable for the scientific goals of the primordial B-mode detection. Nevertheless, previous research has shown that the construction of large-aperture telescopes has significant implications for other scientific goals [62].

In Table IV, we compare the marginal effects on the constraining capacity of n_s and r when the noise level of NHT is reduced. We do not show the $n_s - r$ panel to avoid possible misunderstandings as a forecast paper.

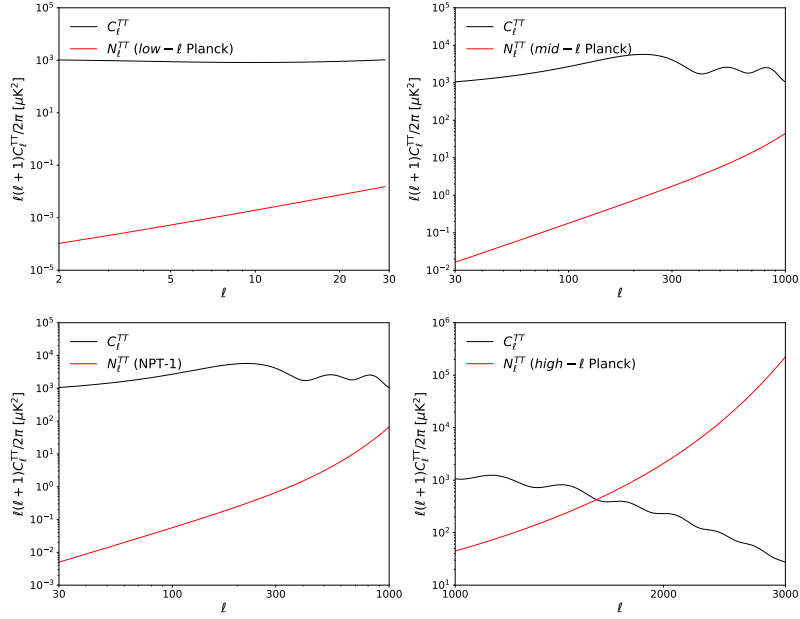


FIG. 3. TT power spectra of the joint likelihood. The black lines represent the power spectra of the fiducial signals, while the red lines indicate the noise power spectra.

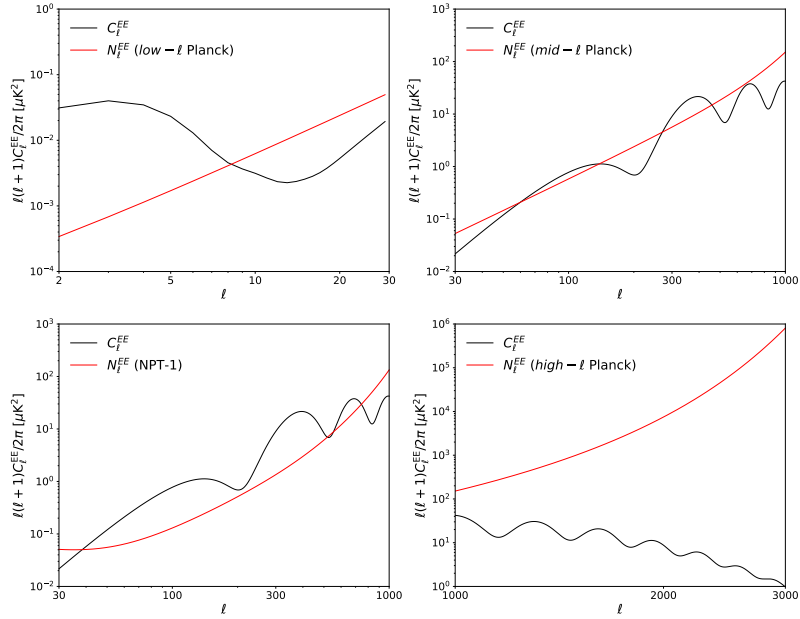


FIG. 4. EE power spectra of the joint likelihood. The black lines represent the power spectra of the fiducial signals, while the red lines indicate the noise power spectra.

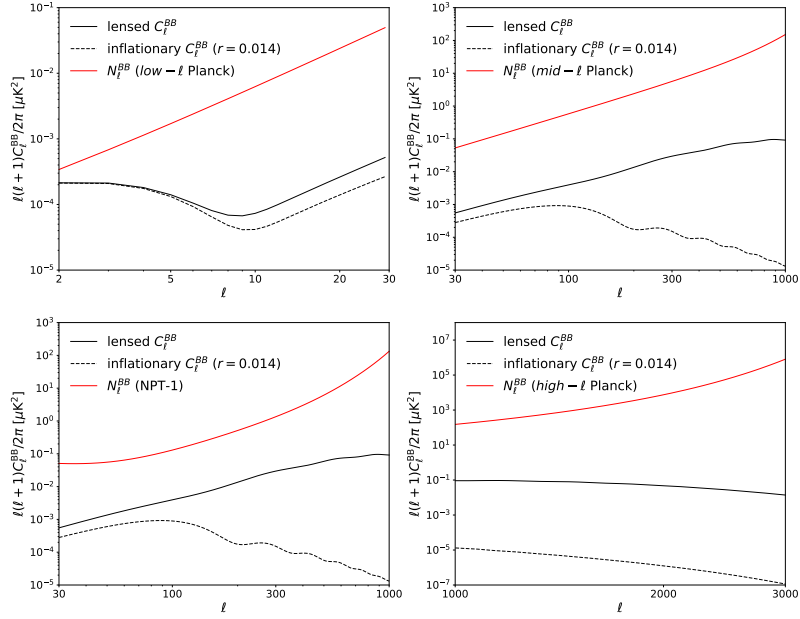


FIG. 5. BB power spectra of the joint likelihood. The solid black lines represent the fiducial lensed BB power spectra, and the dashed black lines represent the fiducial BB power spectra induced by primordial PGWs, with a baseline tensor-to-scalar ratio $r = 0.014$.

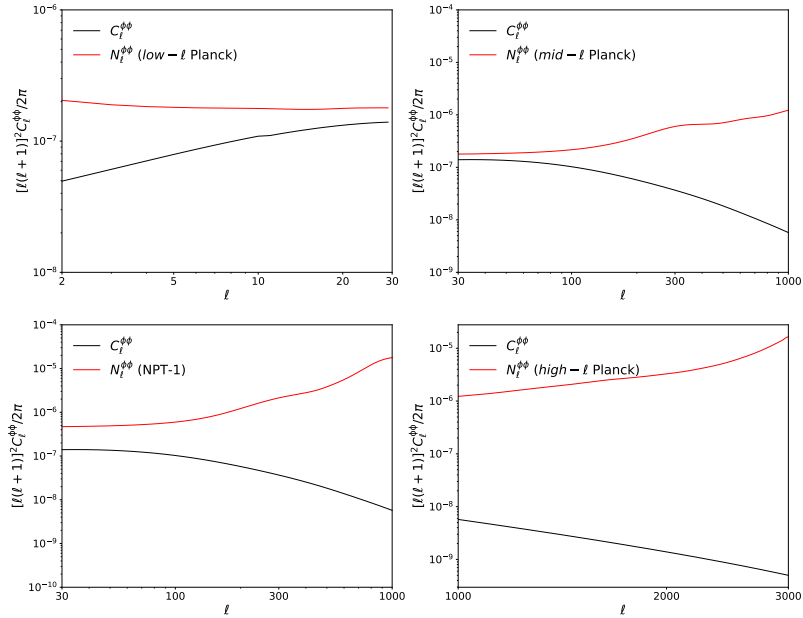
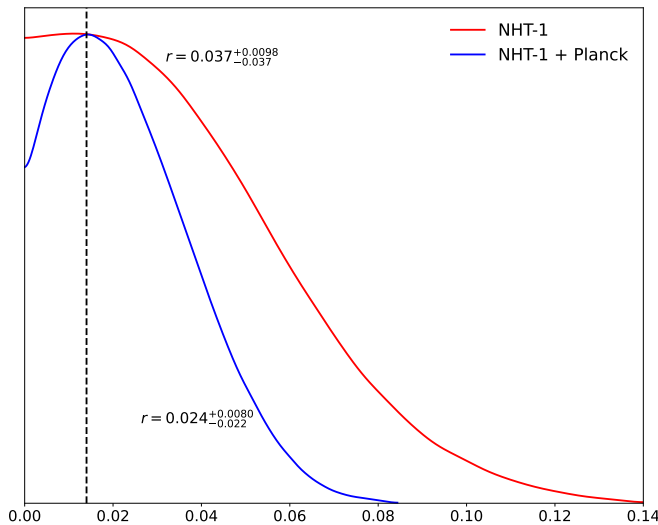
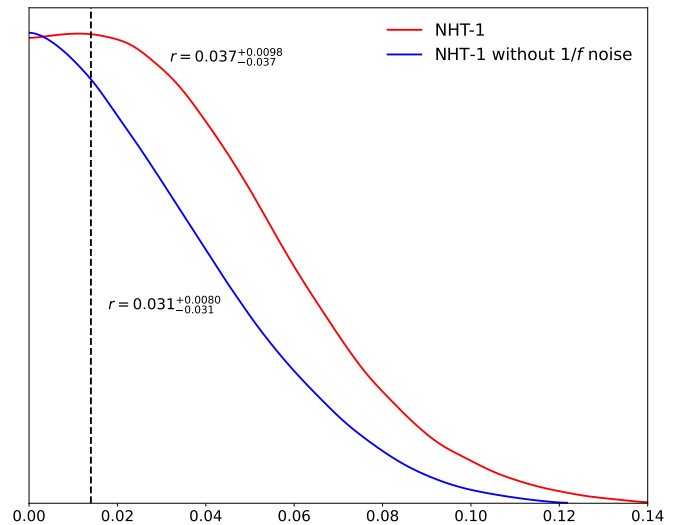


FIG. 6. lensing power spectra of the joint likelihood. The black lines represent the power spectra of the reference signals, generated using Boltzmann code CLASS [59], while the red lines represent the noise power spectra.

Channel (GHz)	FWHM (arcmin)	ΔT ($\mu\text{K}\cdot\text{arcmin}$)	ΔP ($\mu\text{K}\cdot\text{arcmin}$)
1. low- ℓ <i>Planck</i> , $\ell_{\min} = 2$, $\ell_{\max} = 29$, $f_{\text{sky}} = 0.57$			
100	10.0	68.1	42.6
143	7.1	109.4	81.3
2. mid- ℓ <i>Planck</i> , $\ell_{\min} = 30$, $\ell_{\max} = 1000$, $f_{\text{sky}} = 0.47$			
100	10.0	68.1	42.6
143	7.1	109.4	81.3
3. NHT-1, $\ell_{\min} = 30$, $\ell_{\max} = 1000$, $f_{\text{sky}} = 0.1$			
95	19.0	28.3	40.0
150	11.0	28.3	40.0
4. high- ℓ <i>Planck</i> , $\ell_{\min} = 1001$, $\ell_{\max} = 3000$, $f_{\text{sky}} = 0.57$			
100	10.0	68.1	42.6
143	7.1	109.4	81.3

TABLE III. Summary of the joint mock data

FIG. 7. Forecast of the constraint on r using NHT-1 only (red line) and NHT-1 combined with *Planck* (blue line). The vertical line $r = 0.014$ is the fiducial value for r .FIG. 8. Forecasts of the NHT-1 only constraints on r , including (red line) and not including (blue line) $1/f$ noise. The vertical line $r = 0.014$ is the fiducial value for r .

$w_B^{-1/2}$ ($\mu\text{K}\cdot\text{arcmin}$)	40	30	20	10
$\sigma(r)$	0.023	0.015	0.0092	0.0031
$\sigma(n_s)$	0.012	0.011	0.010	0.0096
$\sigma(r)$	0.015	0.013	0.0088	0.0030
$\sigma(n_s)$	0.0040	0.0040	0.0039	0.0038

TABLE IV. The impact of changing noise level $w^{-1/2}$ on parameter constraints. The upper part of the table shows the constraint precision of r under the $\Lambda\text{CDM}+r$ model as $w^{-1/2}$ gradually decreases from 40 $\mu\text{K}\cdot\text{arcmin}$ to 10 $\mu\text{K}\cdot\text{arcmin}$. The lower part presents the expected sensitivity of NHT combined with *Planck* 2018.

our calculations show that reducing noise levels markedly improves the ability to search for PGWs. The improvement of constraints on $\sigma(r)$ from 20 $\mu\text{K}\cdot\text{arcmin}$ to 10 $\mu\text{K}\cdot\text{arcmin}$ is more pronounced than from 40 $\mu\text{K}\cdot\text{arcmin}$ to 20 $\mu\text{K}\cdot\text{arcmin}$, while the ability to reduce the con-

straint on $\sigma(n_s)$ is relatively small. In particular, after being combined with *Planck*, $\sigma(n_s)$ has little to do with the noise level of NHT. This result is easy to understand because *Planck* provides a very precise temperature power spectrum, which has the primary effect on the n_s constraint; The $\sigma(r)$ is directly related to the high-precision polarized B-mode signal, so it is greatly affected by the noise level of NHT. The noise level is inversely proportional to the detection time or the number of detectors, and this result suggests that we should strive to keep the NHT noise level below 10 $\mu\text{K}\cdot\text{arcmin}$, which can be achieved by accumulating data over some years of observation seasons or adding detector modules. For NHT-1 at a noise level of 40 $\mu\text{K}\cdot\text{arcmin}$, even without increasing the number of detectors, it is theoretically possible to reach the level of 10 $\mu\text{K}\cdot\text{arcmin}$ after four years of observation, so our results indicate that the marginal benefit of continuous observation and increasing the number of

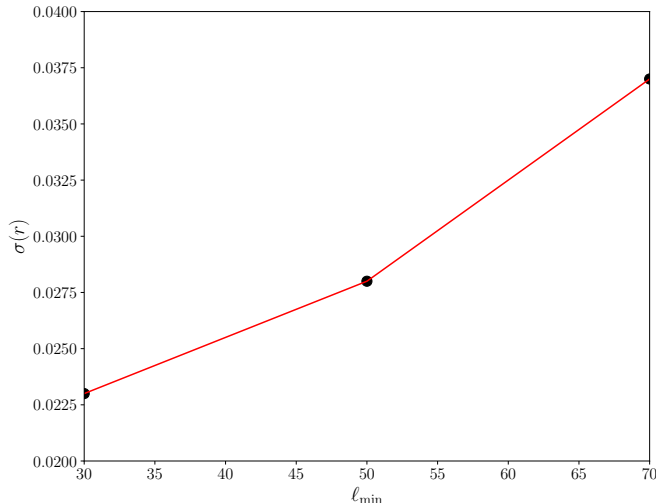


FIG. 9. The impact of changing ℓ_{\min} on the parameter constraints on r .

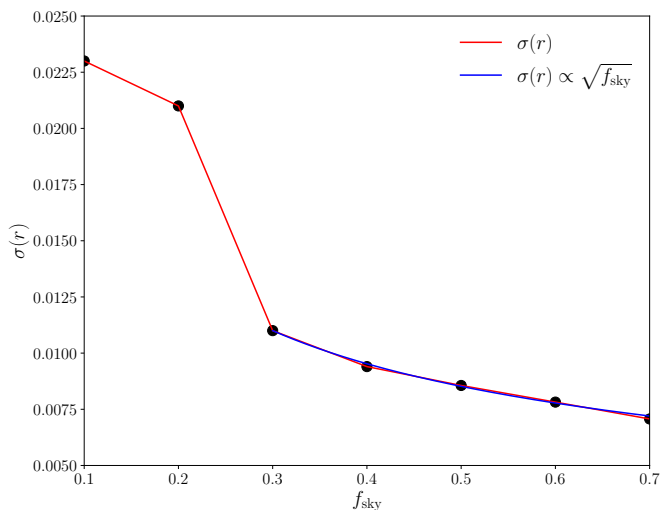


FIG. 10. The impact of changing sky survey coverage f_{sky} on tensor-to-scalar ratio r constraint. The red line is the actual calculated curve, the black dots are the data points; the blue line is the expected curve starting from $f_{\text{sky}} = 0.3$.

detectors is considerable.

In Fig. 10, we show the impact of increasing f_{sky} on improving the accuracy of the constraint on r with NHT only. When f_{sky} increases from 0.1 to 0.7, $\sigma(r)$ decreases from 0.023 to 0.0071, demonstrating a significant effect on increasing the constraining sensitivity of r . We also plot the curve of $\sigma(r) \propto \sqrt{f_{\text{sky}}}$ starting from $f_{\text{sky}} = 0.3$

in the figure. The calculated results deviate from this relationship between $f_{\text{sky}} = 0.1$ and $f_{\text{sky}} = 0.3$ because the 1D constraint on r forecasted by NHT-1 is not a standard Gaussian form. In addition, since NHT's sky surveys rely on specific clean sky areas in the northern hemisphere, such significant strategic expectations may not be possible for the construction of NHT. Nevertheless, this finding highlights the high scientific significance of a global network of ground-based CMB telescopes to jointly detect PGWs.

IV. CONCLUSIONS

In this work, we constructed a generic simulated survey data for Northern Hemisphere CMB telescope, NHT, independent of specific pipeline methods, and forecasted its sensitivity to the tensor-to-scalar ratio of PGWs using the MCMC method. Combining NHT data with the mock data from *Planck* 2018, we forecast a sensitivity of $\sigma(r) = 0.015$ and $r < 0.054$ (95% C.L.) for a fiducial model with $r = 0.014$. This is expected to surpass the BICEP2/*Keck* report.

Moreover, we explore how certain instrument parameters can enhance the ability to constrain PGWs. We found that low- ℓ polarization mock data significantly affects $\sigma(r)$, indicating that strict atmospheric noise removal techniques are crucial for improving NHT's ability to constrain PGWs.

Additionally, our calculations show that reducing noise levels significantly enhances the ability to search for PGWs. The improvement from $20 \mu\text{K} \cdot \text{arcmin}$ to $10 \mu\text{K} \cdot \text{arcmin}$ is more substantial than from $40 \mu\text{K} \cdot \text{arcmin}$ to $20 \mu\text{K} \cdot \text{arcmin}$, indicating significant marginal effects from continuous observation and increased detector numbers.

Furthermore, we study the impact of increasing sky coverage f_{sky} and show that it significantly affects the constraining sensitivity on r . Since NHT's sky surveys rely on specific clean sky areas, achieving these strategic expectations may be challenging. However, this highlights the high scientific significance of a global network of ground-based CMB telescopes for joint PGW detection.

In summary, based on realistic and feasible experimental parameters, NHT has the scientific potential to achieve leading international constraints on PGWs and make continuous progress. Additionally, due to the lack of high-precision ground-based CMB data in the northern sky, the addition of NHT can supplement existing data and independently verify or combine with future experiments like BICEP ARRAY or CMB-S4. We analyzed and demonstrated through mock data that constructing NHT holds significant scientific importance for the near-future detection of PGWs.

ACKNOWLEDGMENTS

We are grateful to Hong Li, Siyu Li, Yang Liu, Wentao Luo, Toshiya Namikawa, Larissa Santos and Rui Shi for valuable communications. This work is supported in part by the National Key R&D Program of China (2021YFC2203100), CAS Young Interdisciplinary Innovation Team (JCTD-2022-20), NSFC (12261131497, 11653002, 12003029), 111 Project for ‘‘Observational and Theoretical Research on Dark Matter and Dark Energy’’

(B23042), Fundamental Research Funds for Central Universities, CSC Innovation Talent Funds, USTC Fellowship for International Cooperation, USTC Research Funds of the Double First-Class Initiative, CAS project for young scientists in basic research (YSBR-006). Kavli IPMU is supported by World Premier International Research Center Initiative (WPI), MEXT, Japan. We acknowledge the use of computing facilities of astronomy department, as well as the clusters LINDA & JUDY of the particle cosmology group at USTC.

-
- [1] A. A. Starobinsky, A new type of isotropic cosmological models without singularity, *Physics Letters B* **91**, 99 (1980).
- [2] D. Kazanas, Dynamics of the universe and spontaneous symmetry breaking, *Astrophysical Journal, Part 2-Letters to the Editor*, vol. 241, Oct. 15, 1980, p. L59-L63. **241**, L59 (1980).
- [3] K. Sato, First-order phase transition of a vacuum and the expansion of the universe, *Monthly Notices of the Royal Astronomical Society* **195**, 467 (1981).
- [4] A. H. Guth, Inflationary universe: A possible solution to the horizon and flatness problems, *Phys. Rev. D* **23**, 347 (1981).
- [5] A. D. Linde, A new inflationary universe scenario: A possible solution of the horizon, flatness, homogeneity, isotropy and primordial monopole problems, *Physics Letters B* **108**, 389 (1982).
- [6] A. D. Linde, Chaotic inflation, *Physics Letters B* **129**, 177 (1983).
- [7] A. Albrecht and P. J. Steinhardt, Cosmology for Grand Unified Theories with Radiatively Induced Symmetry Breaking, *Phys. Rev. Lett.* **48**, 1220 (1982).
- [8] V. F. Mukhanov and G. V. Chibisov, Quantum fluctuations and a nonsingular universe, *ZhETF Pisma Redaktsii* **33**, 549 (1981).
- [9] S. W. Hawking, The development of irregularities in a single bubble inflationary universe, *Physics Letters B* **115**, 295 (1982).
- [10] A. H. Guth and S. Y. Pi, Fluctuations in the New Inflationary Universe, *Phys. Rev. Lett.* **49**, 1110 (1982).
- [11] A. A. Starobinsky, Dynamics of phase transition in the new inflationary universe scenario and generation of perturbations, *Physics Letters B* **117**, 175 (1982).
- [12] J. M. Bardeen, J. R. Bond, N. Kaiser, and A. S. Szalay, The Statistics of Peaks of Gaussian Random Fields, *Astrophys. J.* **304**, 15 (1986).
- [13] V. F. Mukhanov, Gravitational Instability of the Universe Filled with a Scalar Field, *JETP Lett.* **41**, 493 (1985).
- [14] U. Seljak and M. Zaldarriaga, Signature of Gravity Waves in the Polarization of the Microwave Background, *Phys. Rev. Lett.* **78**, 2054 (1997), arXiv:astro-ph/9609169 [astro-ph].
- [15] M. Kamionkowski, A. Kosowsky, and A. Stebbins, A Probe of Primordial Gravity Waves and Vorticity, *Phys. Rev. Lett.* **78**, 2058 (1997), arXiv:astro-ph/9609132 [astro-ph].
- [16] W. Hu and M. J. White, A CMB polarization primer, *New Astron.* **2**, 323 (1997), arXiv:astro-ph/9706147 [astro-ph].
- [17] N. Aghanim *et al.* (Planck), Planck 2018 results. VI. Cosmological parameters, *Astron. Astrophys.* **641**, A6 (2020), arXiv:1807.06209 [astro-ph.CO].
- [18] Y. Akrami *et al.* (Planck), Planck 2018 results. X. Constraints on inflation, *Astron. Astrophys.* **641**, A10 (2020), arXiv:1807.06211 [astro-ph.CO].
- [19] P. A. R. Ade *et al.* (BICEP, Keck), Improved Constraints on Primordial Gravitational Waves using Planck, WMAP, and BICEP/Keck Observations through the 2018 Observing Season, *Phys. Rev. Lett.* **127**, 151301 (2021), arXiv:2110.00483 [astro-ph.CO].
- [20] S. Dahal *et al.*, The CLASS 150/220 GHz Polarimeter Array: Design, Assembly, and Characterization, *J. Low Temp. Phys.* **199**, 289 (2020), arXiv:1908.00480 [astro-ph.IM].
- [21] A. Suzuki *et al.* (POLARBEAR), The POLARBEAR-2 and the Simons Array Experiment, *J. Low Temp. Phys.* **184**, 805 (2016), arXiv:1512.07299 [astro-ph.IM].
- [22] T. Louis *et al.* (ACTPol), The Atacama Cosmology Telescope: Two-Season ACTPol Spectra and Parameters, *JCAP* **06**, 031, arXiv:1610.02360 [astro-ph.CO].
- [23] J. E. Carlstrom *et al.*, The 10 Meter South Pole Telescope, *Publ. Astron. Soc. Pac.* **123**, 568 (2011), arXiv:0907.4445 [astro-ph.IM].
- [24] M. Kamionkowski and E. D. Kovetz, The Quest for B Modes from Inflationary Gravitational Waves, *Ann. Rev. Astron. Astrophys.* **54**, 227 (2016), arXiv:1510.06042 [astro-ph.CO].
- [25] K. Abazajian *et al.* (CMB-S4), CMB-S4: Forecasting Constraints on Primordial Gravitational Waves, *Astrophys. J.* **926**, 54 (2022), arXiv:2008.12619 [astro-ph.CO].
- [26] Y.-F. Cai and X. Zhang, Probing the origin of our universe through primordial gravitational waves by Ali CMB project, *Science China Physics, Mechanics, and Astronomy* **59**, 178 (2016), arXiv:1605.01840 [astro-ph.IM].
- [27] Y.-P. Li, Y. Liu, S.-Y. Li, H. Li, and X. Zhang, Tibet’s ali: a new window to detect the cmb polarization, arXiv preprint (2017), arXiv:1709.09053 [astro-ph.IM].
- [28] H. Li *et al.*, Probing Primordial Gravitational Waves: Ali CMB Polarization Telescope, *Natl. Sci. Rev.* **6**, 145 (2019), arXiv:1710.03047 [astro-ph.CO].
- [29] U. Fuskeland *et al.*, B-mode polarization forecasts for GreenPol, *Astron. Astrophys.* **684**, A128 (2024), arXiv:2306.13043 [astro-ph.CO].
- [30] M. G. Bosilovich, *MERRA-2: Initial evaluation of the climate* (National Aeronautics and Space Administration, Goddard Space Flight Center, 2015).
- [31] H. Li, S.-Y. Li, Y. Liu, Y.-P. Li, and X. Zhang, Tibet’s

- window on primordial gravitational waves, *Nature Astronomy* **2**, 104 (2018), [arXiv:1802.08455 \[astro-ph.IM\]](#).
- [32] H. K. Eriksen, A. J. Banday, K. M. Górski, and P. B. Lilje, On Foreground Removal from the Wilkinson Microwave Anisotropy Probe Data by an Internal Linear Combination Method: Limitations and Implications, *Astrophys. J.* **612**, 633 (2004), [arXiv:astro-ph/0403098 \[astro-ph\]](#).
- [33] M. Tegmark, A. de Oliveira-Costa, and A. J. Hamilton, High resolution foreground cleaned CMB map from WMAP, *Phys. Rev. D* **68**, 123523 (2003), [arXiv:astro-ph/0302496 \[astro-ph\]](#).
- [34] D. Maino, A. Farusi, C. Baccigalupi, F. Perrotta, A. J. Banday, L. Bedini, C. Burigana, G. De Zotti, K. M. Gorski, and E. Salerno, All-sky astrophysical component separation with fast independent component analysis (fastica), *Mon. Not. Roy. Astron. Soc.* **334**, 53 (2002), [arXiv:astro-ph/0108362](#).
- [35] J. Delabrouille, J. F. Cardoso, and G. Patanchon, Multi-detector multi-component spectral matching and applications for CMB data analysis, *Mon. Not. Roy. Astron. Soc.* **346**, 1089 (2003), [arXiv:astro-ph/0211504](#).
- [36] J.-F. Cardoso, M. Le Jeune, J. Delabrouille, M. Betoule, and G. Patanchon, Component separation with flexible models—application to multichannel astrophysical observations, *IEEE Journal of Selected Topics in Signal Processing* **2**, 735 (2008), [arXiv:0803.1814 \[astro-ph\]](#).
- [37] H. K. Eriksen, J. B. Jewell, C. Dickinson, A. J. Banday, K. M. Górski, and C. R. Lawrence, Joint Bayesian Component Separation and CMB Power Spectrum Estimation, *Astrophys. J.* **676**, 10 (2008), [arXiv:0709.1058 \[astro-ph\]](#).
- [38] F. Stivoli, J. Grain, S. M. Leach, M. Tristram, C. Baccigalupi, and R. Stompor, Maximum likelihood, parametric component separation and cmb b-mode detection in suborbital experiments, *Monthly Notices of the Royal Astronomical Society* **408**, 2319 (2010), [arXiv:1004.4756 \[astro-ph.CO\]](#).
- [39] E. Martínez-González, J. M. Diego, P. Vielva, and J. Silk, CMB power spectrum estimation and map reconstruction with the expectation - Maximization algorithm, *Mon. Not. Roy. Astron. Soc.* **345**, 1101 (2003), [arXiv:astro-ph/0302094 \[astro-ph.CO\]](#).
- [40] S. M. Leach *et al.*, Component separation methods for the Planck mission, *Astron. Astrophys.* **491**, 597 (2008), [arXiv:0805.0269 \[astro-ph\]](#).
- [41] R. Fernández-Cobos, P. Vielva, R. B. Barreiro, and E. Martínez-González, Multiresolution internal template cleaning: an application to the wilkinson microwave anisotropy probe 7-yr polarization data, *Monthly Notices of the Royal Astronomical Society* **420**, 2162 (2012), [arXiv:1106.2016 \[astro-ph.CO\]](#).
- [42] D. Adak, A. Sen, S. Basak, J. Delabrouille, T. Ghosh, A. Rotti, G. Martínez-Solaèche, and T. Souradeep, B-mode forecast of CMB-Bhārat, *Mon. Not. Roy. Astron. Soc.* **514**, 3002 (2022), [arXiv:2110.12362 \[astro-ph.CO\]](#).
- [43] N. Krachmalnicoff *et al.* (LiteBIRD), In-flight polarization angle calibration for LiteBIRD: blind challenge and cosmological implications, *JCAP* **01** (01), 039, [arXiv:2111.09140 \[astro-ph.CO\]](#).
- [44] Z. Zhang, Y. Liu, S.-Y. Li, D.-L. Wu, H. Li, and H. Li, Efficient ILC analysis on polarization maps after EB leakage correction, *JCAP* **22**, 044, [arXiv:2109.12619 \[astro-ph.CO\]](#).
- [45] A. Carones, M. Migliaccio, D. Marinucci, and N. Vittorio, Analysis of Needlet Internal Linear Combination performance on B-mode data from sub-orbital experiments, *Astron. Astrophys.* **677**, A147 (2023), [arXiv:2208.12059 \[astro-ph.CO\]](#).
- [46] S. Ghosh *et al.*, Performance forecasts for the primordial gravitational wave detection pipelines for AliCPT-1, *JCAP* **10**, 063, [arXiv:2205.14804 \[astro-ph.CO\]](#).
- [47] J. Dou, S. Ghosh, L. Santos, and W. Zhao, Foreground removal with ILC methods for AliCPT-1, *JCAP* **05**, 006, [arXiv:2310.19627 \[astro-ph.CO\]](#).
- [48] P. Ade *et al.* (Simons Observatory), The Simons Observatory: Science goals and forecasts, *JCAP* **02**, 056, [arXiv:1808.07445 \[astro-ph.CO\]](#).
- [49] L. Santos, J. Yao, L. Zhang, S. Ghosh, P. Zhang, W. Zhao, T. Villela, J. Chen, and J. Delabrouille, Testing the analytical blind separation method in simulated CMB polarization maps, *Astron. Astrophys.* **650**, A65 (2021), [arXiv:1908.07862 \[astro-ph.CO\]](#).
- [50] M. Remazeilles, A. Rotti, and J. Chluba, Peeling off foregrounds with the constrained moment ILC method to unveil primordial CMB *B*-modes, *Mon. Not. Roy. Astron. Soc.* **503**, 2478 (2021), [arXiv:2006.08628 \[astro-ph.CO\]](#).
- [51] J. Han *et al.*, Forecasts of CMB lensing reconstruction of AliCPT-1 from the foreground cleaned polarization data, *JCAP* **04**, 063, [arXiv:2303.05705 \[astro-ph.CO\]](#).
- [52] L. Knox, Determination of inflationary observables by cosmic microwave background anisotropy experiments, *Phys. Rev. D* **52**, 4307 (1995), [arXiv:astro-ph/9504054 \[astro-ph\]](#).
- [53] J. Errard, S. M. Feeney, H. V. Peiris, and A. H. Jaffe, Robust forecasts on fundamental physics from the foreground-obscured, gravitationally-lensed CMB polarization, *JCAP* **03**, 052, [arXiv:1509.06770 \[astro-ph.CO\]](#).
- [54] T. Okamoto and W. Hu, Cosmic microwave background lensing reconstruction on the full sky, *Phys. Rev. D* **67**, 083002 (2003), [arXiv:astro-ph/0301031 \[astro-ph\]](#).
- [55] <https://github.com/dhanson/quicklens>.
- [56] T. Brinckmann, D. C. Hooper, M. Archidiacono, J. Lesgourgues, and T. Sprenger, The promising future of a robust cosmological neutrino mass measurement, *JCAP* **01**, 059, [arXiv:1808.05955 \[astro-ph.CO\]](#).
- [57] T. Brinckmann and J. Lesgourgues, MontePython 3: Boosted MCMC sampler and other features, *Physics of the Dark Universe* **24**, 100260 (2019), [arXiv:1804.07261 \[astro-ph.CO\]](#).
- [58] B. Audren, J. Lesgourgues, K. Benabed, and S. Prunet, Conservative constraints on early cosmology with monte python, *Journal of Cosmology and Astroparticle Physics* **2013** (02), 001, [arXiv:1210.7183 \[astro-ph.CO\]](#).
- [59] D. Blas, J. Lesgourgues, and T. Tram, The cosmic linear anisotropy solving system (class). part ii: Approximation schemes, *Journal of Cosmology and Astroparticle Physics* **2011** (07), 034, [arXiv:1104.2933 \[astro-ph.CO\]](#).
- [60] A. Gelman and D. B. Rubin, Inference from Iterative Simulation Using Multiple Sequences, *Statist. Sci.* **7**, 457 (1992).
- [61] P. A. R. Ade *et al.* (BICEP2, Keck Array), BICEP2 / Keck Array x: Constraints on Primordial Gravitational Waves using Planck, WMAP, and New BICEP2/Keck Observations through the 2015 Season, *Phys. Rev. Lett.* **121**, 221301 (2018), [arXiv:1810.05216 \[astro-ph.CO\]](#).
- [62] D. Zhang, J.-R. Li, J. Li, J. Yang, Y. Zhang, Y.-F. Cai, W. Fang, and C. Feng, Future Prospects on Constraining Neutrino Cosmology with the Ali CMB Polarization Telescope, *Astrophys. J.* **946**, 32 (2023), [arXiv:2112.10539](#)

[astro-ph.CO].